Meteorol. Atmos. Phys. 64, 187–201 (1997)

Meteorology and Atmospheric Physics

[1] Center for Air Sea Technology, Mississippi State University, Stennis Space Center, Mississippi, U.S.A.
[2] Department of Atmospheric and Oceanic Sciences, and Center for Climate and Global Change Research, McGill University, Montreal, P. Q. Canada
[3] Centre de recherche en calcul appliqué Montréal, Québec, Canada
[4] Rosentiel School of Marine Science, University of Miami, Miami, Florida, U.S.A.

A High Resolution Numerical Study of Gulf of Mexico Fronts and Eddies

D. E. Dietrich[1], **C. A. Lin**[2,3], **A. Mestas-Nunez**[1], and **D.-S. Ko**[4]

With 10 Figures

Received December 16, 1996
Revised June 22, 1997

Summary

The Gulf of Mexico (GOM) circulation is simulated using the DieCAST ocean model, with a horizontal resolution of 1/12° and 20 vertical layers. The results compare well with observations of both large and small scale features, including Loop Current frontal occlusions associated with frontal eddies. The simulation is carried out without any data assimilation. The frontal eddies tend to be spaced at about 90° intervals around the Loop Current, leading to a Loop Current head shaped like a square with rounded corners. The pattern rotates as the eddies circle the Loop, and frontal eddies elongate as they squeeze through the Florida Strait. Major warm core eddies separate regularly from the Loop Current and propagate to the western GOM. Old warm core eddies in the western Gulf dissipate through bottom drag effects, which also generate cyclonic parasitic eddies. Newly arrived warm core eddies merge with old ones in the western GOM. Recently separated elongated Loop Current eddies can rotate and reattach temporarily to the Loop Current. The barotropic flow component develops eddies between the main separated warm core eddy and the Loop Current due to eastward dispersion, as the main eddy itself propagates westward into the Gulf.

1. Introduction

There has been a large number of observational studies of the Gulf of Mexico circulation. The Gulf is a semi-enclosed basin with well known inflow/outflow boundary conditions. GEOSAT satellite surface height observations provide a good picture of the Gulf, because surface height variations are large and associated with large scale eddies that dominate deep regions. Even the smaller scale shelf dynamics are being observed in detail, using drifters and other in situ measurements, in the LATEX Program. The general circulation is dominated by the Loop Current and eddies which are shed off the Current. The Gulf is large enough to include major features of basin scale ocean dynamics, and is yet small enough to model with high resolution on workstations. It is thus a good region to compare and validate numerical models.

There is evidence of significant air-sea interaction over the Gulf which gives rise to extratropical and tropical storms. Lewis and Hsu (1992) presented observations showing that winter cyclogenesis over the northwestern Gulf may be enhanced by the mesoscale horizontal baroclinicity between the deeper, warmer Gulf and the cooler inner shelf region. There is also observational evidence that the Loop Current and its warm core rings are heat and moisture sources

from which a nearby, slowly moving tropical disturbance can extract energy.

In a pioneering modelling study, Hurlburt and Thompson (1980) examined the Loop Current and eddy shedding over a wide range of model parameters. Their theory was based on the conservation of absolute potential vorticity, and the results showed that the basic eddy shedding mechanism is barotropic in nature. There have been other studies of the eddy shedding phenomenon since then. Lewis and Kirwan (1987) reported Wallcraft's (1986) simulations using the Hurlburt and Thompson model of an eddy shedding sequence. Using a 2-layer primitive equation model, Smith (1986) examined the interaction of Loop Current eddies with topography in the western Gulf. He identified two dynamical regimes depending on the lower layer rotational strength of the eddy. However, the topographic β-effect does not seem to steer the simulated anticyclones along topographic contours, as suggested by observational studies.

Blumberg and Mellor (1985) used a sigma coordinate free surface model with a turbulence closure scheme to model the Gulf circulation. Wind stress, surface heating and salinity effects were included in a 1-year simulation. The results showed some of the basic features of the Gulf circulation. The model did not show eddy shedding at a resolution of 50 km, which might be due to the large eddy diffusivities used.

Arango and Reid (1991) used a generalized reduced gravity model in isopycnic coordinates to simulate the eddy shedding process. In addition to the anticyclonic eddy, the simulations also show the presence of the cyclonic eddy in the shear zone between Campeche Bank and the West Florida Shelf. The latter eddy has been observed in eddy shedding sequence (Vukovich and Maul, 1985).

Our Arakawa C-grid SOMS model (Sandia Ocean Modeling System: Dietrich et al., 1987; Dietrich, 1992) and Arakawa A-grid DieCAST model (Dietrich/Center for Air Sea Technology: Dietrich et al., 1994; hereafter referred to as DKY) have previously been applied to the Gulf of Mexico including the northwestern Caribbean Sea. The DieCAST and SOMS models combine features of the standard A- and C-grid approaches to strengthen their respective weaknesses in treating the pressure gradient/divergence terms and the Coriolis terms. These A- and C-grid algorithms converge to the same results with increasing resolution in a prototype ocean problem (Dietrich et al., 1990), with 20 km resolution being adequate for the main deep water features of the idealized flat bottom basin-scale simulations performed. For the Gulf of Mexico (GOM), the SOMS and DieCAST models give remarkably similar results with 20 km resolution (Dietrich and Ko, 1994).

Dietrich and Lin (1994; hereafter referred to as DL) studied GOM Loop Current eddy shedding using the SOMS model. The results compare well with observations, and are consistent with barotropic theory and model results of Hurlburt and Thompson (1980). Together with a scaling analysis of the quasi-geostrophic omega equation for the vertical motion, DL's modelling results also show significant eddy shedding effects from reasonable stratification variations, thus suggesting seasonal cycle effects may be significant. DKY studied the effects of diffusivity and Caribbean Sea inflows using higher vertical resolution than that of DL. Various effects were examined, including the nature of western GOM parasitic eddies. DKY also discussed mechanisms for parasitic eddies in the western Gulf, and showed that the results compare well with observations.

The results from Case B3 of DKY, with Caribbean Sea inflows based on observations reported by Schmitz and Richardson (1991), compare well with a multitude of observations. These include GEOSAT root-mean-square sea surface height anomaly; mean eddy shedding period; dynamics of cyclonic parasitic eddies in the western Gulf; mean thermocline and vertical empirical orthogonal functions; cross-shelfbreak spurts; the development of a shallow pool of cool water inside the Loop Current during its northward penetration. Further theoretical analysis of the results shows that secondary Ekman-like boundary layer flows associated with bottom drag augment shelfbreak fronts and cyclonic parasitic eddies, and a nonlinear critical area mechanism favours the development of large amplitude parasitic eddies under certain conditions. In addition, boundary current vorticity separation dynamics can lead to blocking cyclonic eddies which can arrest the Loop Current northward penetration and eddy shed-

ding when the flow amplitude is increased. Finally, the use of eddy viscosities larger than about $100\,m^2\,s^{-1}$ eliminates parasitic eddies in the western GOM, as their formation involves boundary current separation, which is a high Reynolds number flow phenomon.

The earlier studies with the SOMS model did not include wind forcing or surface thermodynamic forcing, as the flow was forced entirely by inflow from the Carribean Sea. In this study, we use the DieCAST model and include these secondary forcing effects. We also increase the horizontal resolution from 20 km (approx. 1/5°) to 1/12°, while using the same shelf-resolving 20-level vertical resolution as in DKY. The present higher resolution is adequate for the DieCAST model to simulate realistically intense parasitic and Loop Current frontal eddies, leading to frontal occlusions, which is a significant improvement over the lower resolution DKY results.

2. Model Formulation

The governing equations of the DieCAST model are the rigid-lid hydrostatic Boussinesq primitive equations, are as follows:

$$u_t = -p_x/\rho_0 + fv - \nabla\cdot(u\mathbf{V}) + C\nabla^2 u + (K_m u_z)_z \tag{1}$$

$$v_t = -p_y/\rho_0 - fu - \nabla\cdot(v\mathbf{V}) + C\nabla^2 v + (K_m v_z)_z \tag{2}$$

$$T_t = -\nabla\cdot(T\mathbf{V}) + D\nabla^2 T + (K_h T_z)_z \tag{3}$$

$$p_z = \varepsilon g T \tag{4}$$

$$\nabla\cdot\mathbf{V} = 0 \tag{5}$$

The symbols u, v, p, T, t, denote the zonal (x) and meridional (y) velocities, pressure, temperature, and time, respectively; $\mathbf{V}$ is the 3-dimensional velocity field including the vertical (z) motion. Subscripts x, y, z, t, denote partial differentiation with respect to the appropriate parameter. The variable Coriolis parameter is f, while ε, g, ρ_0 are the coefficient of thermal expansion, the gravitational acceleration, and a reference density, respectively; C, D, K_m, K_h are the eddy diffusivities for momentum and heat in the horizontal and vertical. ∇ and ∇^2 are the divergence and Laplacian operators respectively. Equations (1)–(2) are the horizontal momentum equations, (3) is the temperature equation, (4) is the hydrostatic relation, while (5) is the continuity equation for a Bousinessq fluid. Spherical curvilinear terms are included in basin and global scale versions of the DieCAST model.

The model uses a modified Arakawa A-grid formulation. Fourth order approximations are used for the baroclinic pressure gradient and for interpolations between the A- and C-grids to derive a nondivergent advection velocity on the C-grid. This method corresponds to Scheme 3 of Dietrich et al. (1990).

The model parameters are similar to those of Case B3 of DKY (Table 1) except for the following changes. The horizontal resolution is increased from 20 km to 1/12°; eastern Caribbean inflows are moved slightly southward to better reflect the expected distribution based on the Windward Passage location (all other passages are south of the model domain and are represented by the wbc inflow specified at the model southern boundary); surface forcings consisting of climatological January Hellerman winds (Hellerman and Rosenstein, 1983) and Haney restoring (Haney, R. L., 1971) of the top level temperature to the Levitus winter climatology (Levitus, 1982) are used. Such local wind forcing is much less important than the Caribbean inflows except in the relatively weak continental shelf flows, where major currents and eddies do

Table 1. *Model Parameters.*
Inflows (1 Sverdrup = $10^6 m^3 s^{-1}$) are based on observations reported by Schmitz and Richardson (1991). The eastern inflow is derived from a thermal wind balance and concentrated in the upper 500 m. Inflow stratification is given by Levitus Climatology. The model layer iterfaces are: 20, 46, 76, 111, 153, 203, 263, 334, 418, 519, 682, 782, 953, 1160, 1400, 1680, 2030, 2440, and 2920 m

Horizontal diffusivity	Vertical diffusivity	Horizontal resolution	Time step increment	Eastern inflow	wbc inflow
$10\,m^2 s^{-1}$	$1\,cm^2\,s^{-1}$	1/12 deg	40 min	7 Sv	18 Sv

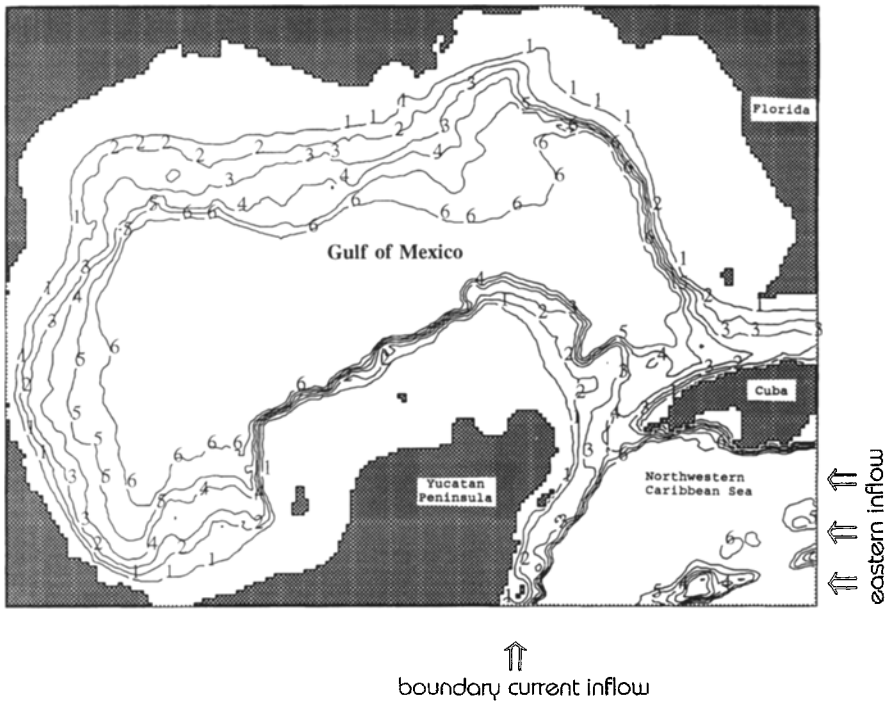

Fig. 1. The Unfiltered bathymetry of the Gulf, as used by the model. The contour interval is 500 m, with the maximum depth truncated at 3500 m. The western boundary current and eastern inflows are indicated

not appear because of strong vorticity constraints. Unfiltered topography is used with depths truncated at 3.5 km, as the use of topographic filters could distort the shelf and shelfbreak dynamics. The model domain, the GOM bathymetry and the inflows used are shown in Fig. 1.

For the present analysis of the GOM circulation, temperature is the only state variable. This is appropriate when deep water formation effects are secondary. Initial and inflow temperatures are derived from the Levitus climatology. A nonlinear equation of state is first used to get the density field from the Levitus climatological temperature and salinity distributions. The density is then related to a "pseudo-temperature" through a linear equation of state with a thermal expansion coefficient of $0.0002\,^{\circ}C^{-1}$. (The pseudo-temperature so obtained is then rescaled to be close to the actual temperature at the surface, which makes it about one degree warmer at depth when using the specified thermal expansion coefficient. It is important to note that the dynamically relevant variable is density, which is correctly represented throughout the water column.) Even freshwater river plume effects, whose density effects are important in shallow continental shelf areas, may be reasonably represented by adjustment of the model pseudotemperature to give appropriate river inflow density. The eastern open boundary inflow horizontal temperature gradient is adjusted to give a surface trapped geostrophic inflow consistent with the observational results of Schmitz and Richardson (1991); the inflow temperature and velocities are taken to be time independent. A barotropic western boundary current inflow of 18 Sv is specified to represent the inflow from the southern Caribbean, resulting in a total Caribbean inflow of 25 Sv. Further details on the inflow specification are given in DL and DKY. There is zero initial flow in the Gulf; the specified inflows are switched on at the first time step of the model simulation.

The lateral heat and momentum diffusivities have a constant value of $10\,m^2\,s^{-1}$. The vertical heat and momentum diffusivities are $1\,cm^2\,s^{-1}$, together with a small additive variable numerical contribution which is dependent on the cell Peclet number; further details are given in DL. Effects of bottom drag are included through the use of a nonlinear drag coefficient of 0.002.

The present simulation was done on a Silicon Graphics workstation with 5 megaflops of computational speed. With 1/12° horizontal resolution and 20 vertical levels, computations

with the 194×146×20 model grid took 24 hours of CPU time for 40 days of GOM simulation. Subsequent tests show that with a single Cray YMP processor, the model runs at 210 megaflops.

3. Results

The results obtained with the high resolution (1/12°) used in the present work provide more details than previous lower resolution studies, especially regarding fronts and frontal eddies. The simulated eddy shedding occurs at approximately days 190, 360, 590, 890, 1080, and 1320. This gives an average eddy shedding period of about 240 days after the second eddy shedding, with an overall variation in the period from 190 to 300 days. This is slightly shorter than the value of 268 days obtained by DKY (their case B3) with a six year simulation. However, as discussed in Section 2, the model parameters are slightly different for the two studies.

Before we investigate the details of the eddy shedding, we first examine the laterally and time averaged distribution of temperature in the vertical. The mean vertical temperature profile compares well with the observations (Fig. 2) as did case B3 of Dietrich and Ko (1994). This shows that the model maintains a realistic thermocline long after intialization from climatology. The latter is calculated from the full history of available winter time GOM data. The model thermocline is a bit too shallow, but lies within one standard deviation of the observed mean distribution. The simulated deep ocean pseudo temperature is about one degree too warm, which correctly corresponds to the slightly warmer pseudo temperature discussed in Section 2 and gives a realistic density profile and thus is dynamically correct. To further assess the simulation of the vertical temperature distribution, we show in Fig. 3 the empirical orthogonal function modes for the model and the observations. The comparison is favourable – even better than the lower resolution Case B3 results.

Even though neither resolution had a sophisticated surface mixed layer model, they are in close agreement with each other and with nature. Apparently even higher order modes are not too sensitive to the mixed layer details. This is the

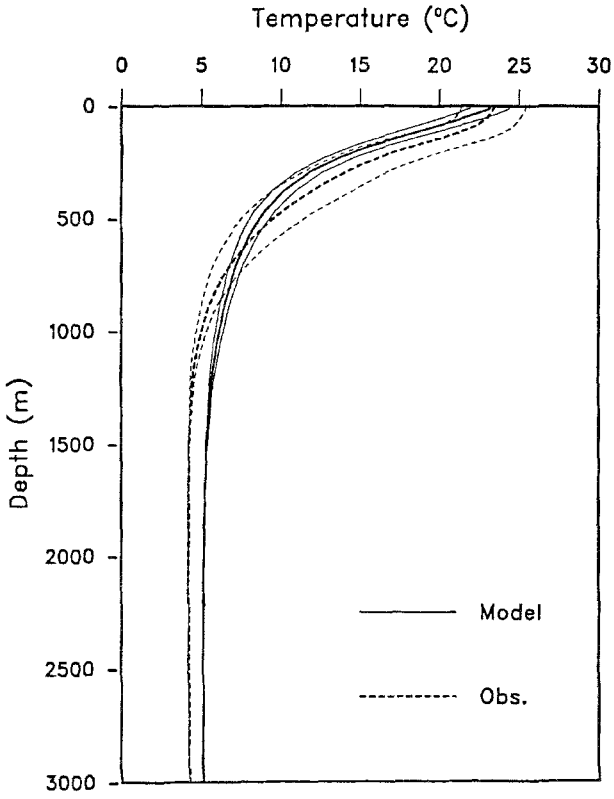

Fig. 2. A comparison of model and observed winter time mean horizontally vertical temperature profiles. The standard deviations for both cases are also shown. The full history of available GOM observed profiles is used in this comparison

first model to show such comparisons. Favorable comparisons demonstrate the model's dynamic similarity to the GOM. The vertical structure of the first two modes, which together account for over 96% of the variance in both the model simulation and observations, is reproduced very well. Even the higher order vertical modes are reproduced with good details. (Note that Figs. 2 and 3 are taken from Dietrich and Ko (1994) published in a journal for numerical methods in fluids, with a readership which is largely different from an oceanographic journal. We repeat these results here to show that the model generates flow statistics which agree well with observations.)

The small differences between the model results and the observations in Figs. 2 and 3 are partly due to the neglect of salinity in our model and the absence of an explicit mixed layer model with synoptic wind events. Nonetheless, the comparisons are improvements over the reason-

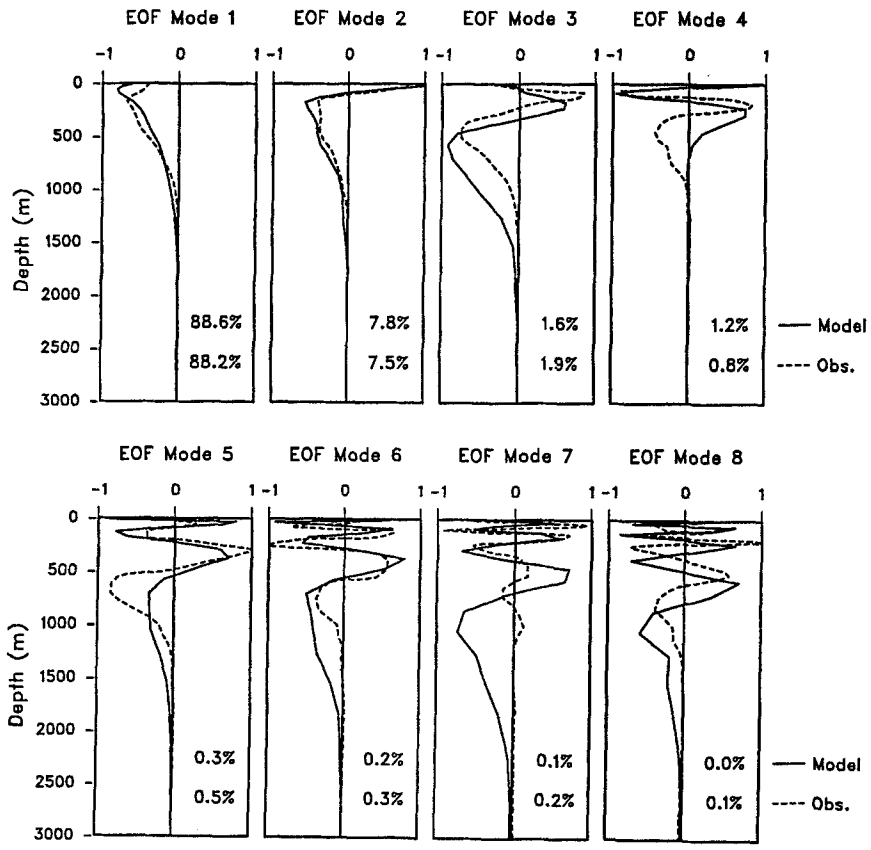

Fig. 3. A comparison of the vertical EOF modes of the model (solid) with those derived from observations (dashed). The percent of total variance represented by each EOF mode is given in each panel, with the observations value located above the model value

able agreement obtained earlier in lower resolution GOM simulations using the SOMS model (Figs. 2 and 3 of DKY). Ko (1992) described the methods used in the present EOF analysis and also showed that the EOF amplitudes are well correlated with GEOSAT sea surface dynamic height observations. This correlation means that a good approximation to the three-dimensional state of the Gulf of Mexico can be derived from a single sea surface height field, through projection on the vertical modes.

Figure 4 shows two satellite snapshots of the temperature field. Similar model snapshots are also shown from near the beginning and end of the model simulation period. The single digit contour label shows only the unit digit. For example, the label "5" denotes a temperature of 25 °C; the contour label is thus the temperature taken at modulo 10. On day 180, there is a narrow wedge of cold water knifing between a separating warm core eddy and the warm water to the south; warm lobes are found in the northeastern and northwestern parts of the separating eddy. In contrast, the snapshot on day 1220 shows a front bifurcation in the northeastern part of the Loop Current and a lobe in the northeastern region; note the lobes are well resolved. These comparisons are noteworthy because:

a) they show that frontal eddies, which are responsible for the Loop Current frontal deformations seen in satellite pictures, are well represented by the model;
b) these two snapshots are from the only model case simulated, and the Loop Current and its frontal eddies obtain a configuration that *could* be compared to the *very few* published snapshots of the Loop Current only *a few* times during the entire model simulation (six eddy shedding events);
c) no data assimilation is used in the model simulations, so the Loop Current frontal eddy details are part of the model's inherent internal dynamics.

To further examine the nature of the front bifurcation of the day 1220 simulation, Fig. 5 shows a time sequence of the surface pressure,

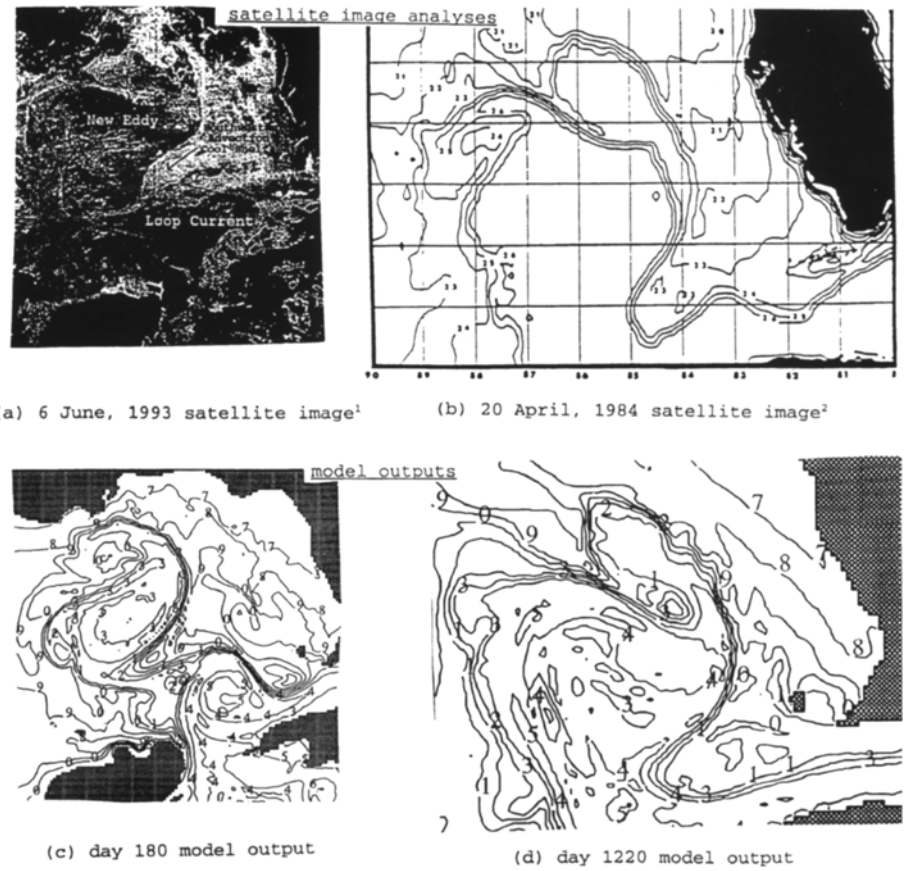

Fig. 4. A comparison of analyzed satellite surface temperatures (top panel) and snapshots of the top layer (10 m depth) model temperature (bottom panel). The single digit contour labels in the model outputs show only the unit digit; thus for example the label "5" denotes a temperature of 250 °C. Plots (b) and (d) are adapted from Dietrich and Ko (1994). (a) 6 June 1993 satellite image, analyzed by Nan Walker (EOS, 27 July, 1993); (b) 20 April 1984 satellite image (p. 87, 'Gulf of Mexico Physical Oceanography Program Final Report, Volume II', MMS publication 87–007, U.S. Department of Interior, Minerals Management Service, Gulf of Mexico OCS Region, New Orleans, LA, published by Evans Waddell and Murray L. Brown); (c) day 180 model output; (d) day 1220 model output

velocity and temperature fields on days 1190, 1200 and 1210. In all pressure field plots, the contour interval is 5 cm of equivalent sea surface height. The absolute values of the contour levels are not dynamically relevant, as only pressure differences need to be considered. (The precise contour label is the model pressure in equivalent sea surface height plus 50 cm, taken at modulo 5.) For the velocity vector field, the maximum speed corresponding to the longest velocity vector is shown.

We see from Fig. 5 that the front bifurcation on day 1220 noted earlier is really an occlusion of the Loop Current front resulting from a strong cyclonic frontal eddy that suddenly develops between days 1190 and 1200 and wraps warm Loop Current water around itself. On the downstream side (i.e., clockwise around the Loop Current front) of the frontal eddy, the Loop Current front first bulges away (westward) from the warm Loop Current core, then continues to wrap around the cyclonic eddy. Positive vorticity advection favors rising motion in this same area according to q-g dynamics, especially as the frontal eddy turns eastward as it gets advected around the Loop by the dominant Loop Current jet (reducing the compensating effect of earth vorticity advection). Thus, vertical temperature advection partially compensates horizontal advection. The DieCAST model's consistent q-g dynamics is discussed by Haney and Dietrich (1996). This eddy is clearly seen located at the

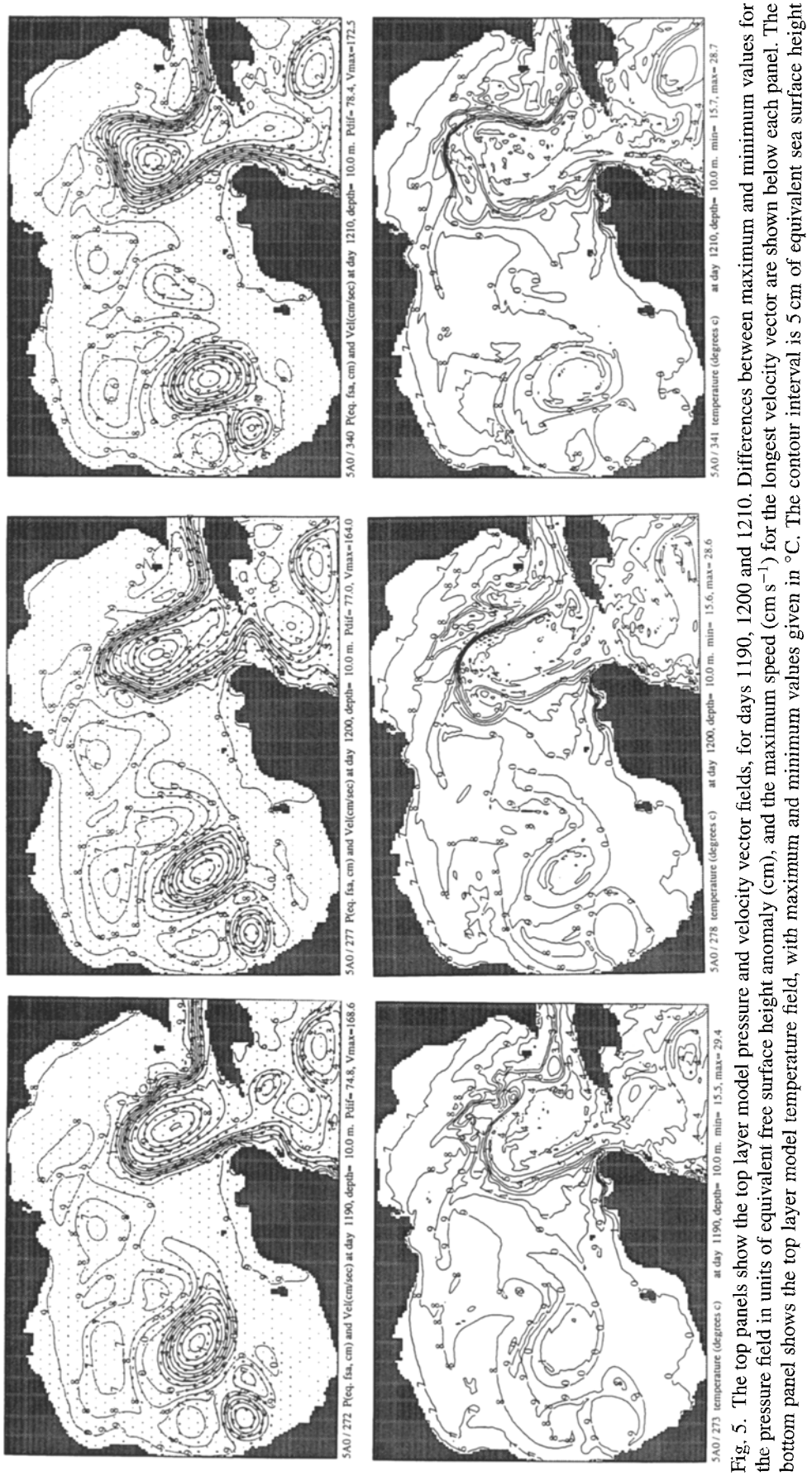

Fig. 5. The top panels show the top layer model pressure and velocity vector fields, for days 1190, 1200 and 1210. Differences between maximum and minimum values for the pressure field in units of equivalent free surface height anomaly (cm), and the maximum speed (cm s^{-1}) for the longest velocity vector are shown below each panel. The bottom panel shows the top layer model temperature field, with maximum and minimum values given in °C. The contour interval is 5 cm of equivalent sea surface height

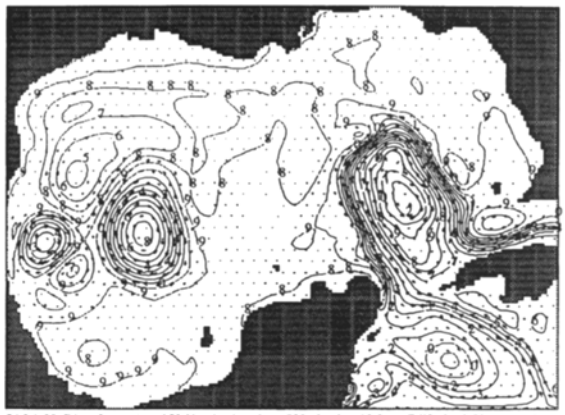

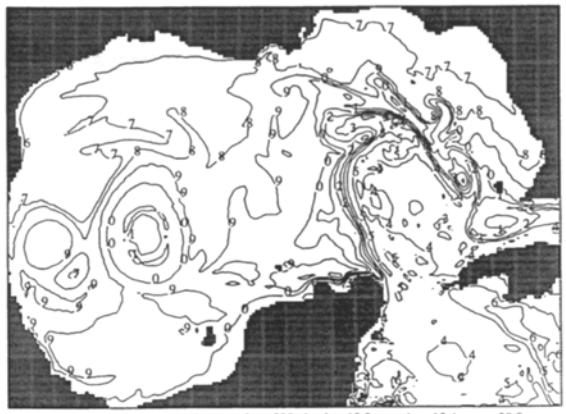

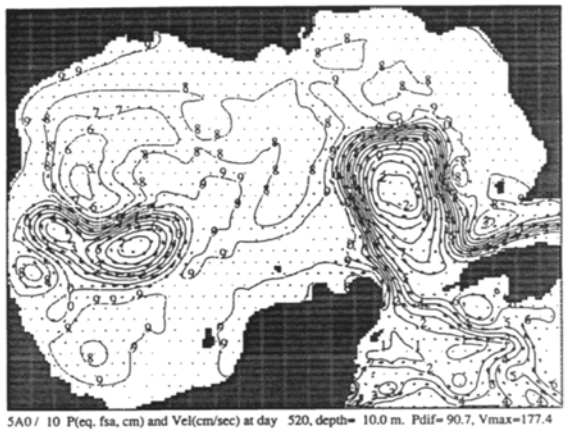

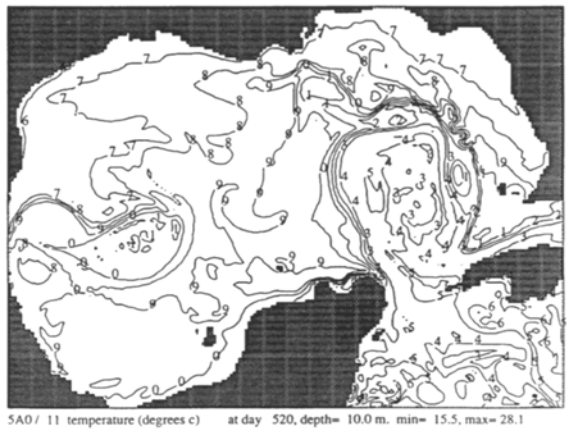

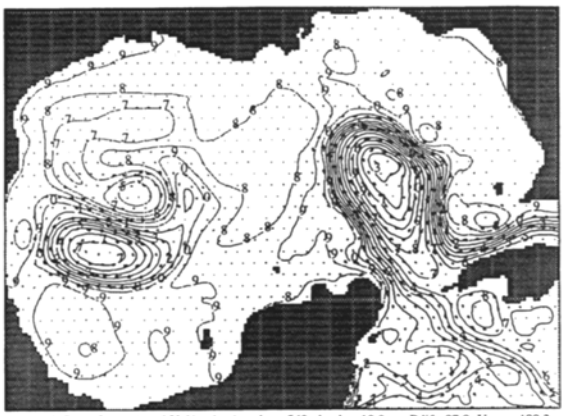

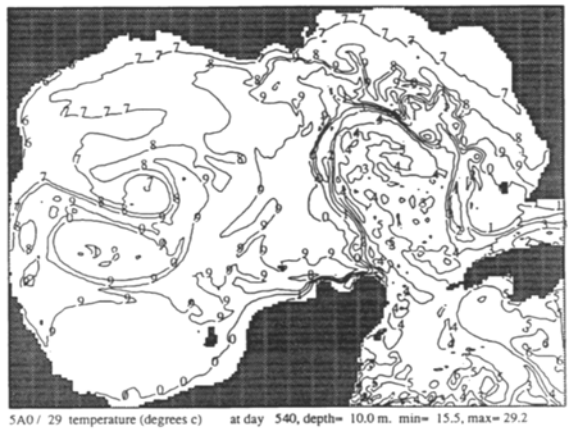

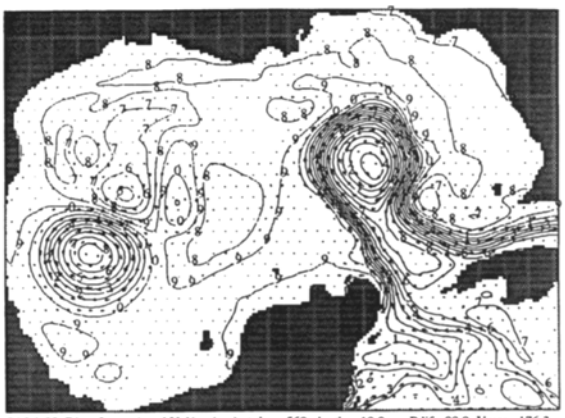

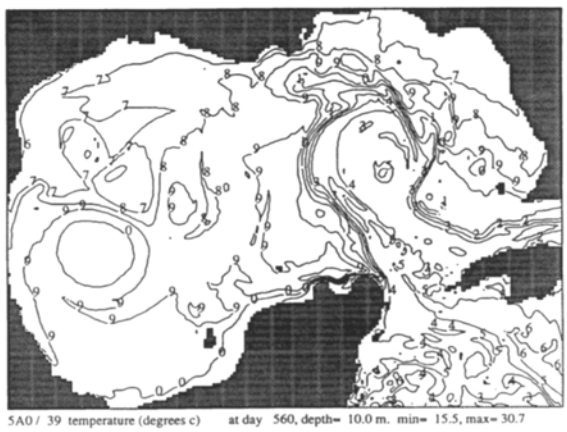

Fig. 6. As Fig. 5, but for the period from days 500 to 560 at 20-day intervals; the left panels show the top layer model pressure and velocity fields, while the right panels show the temperature field. Two old warm core eddies merge in the wester Gulf

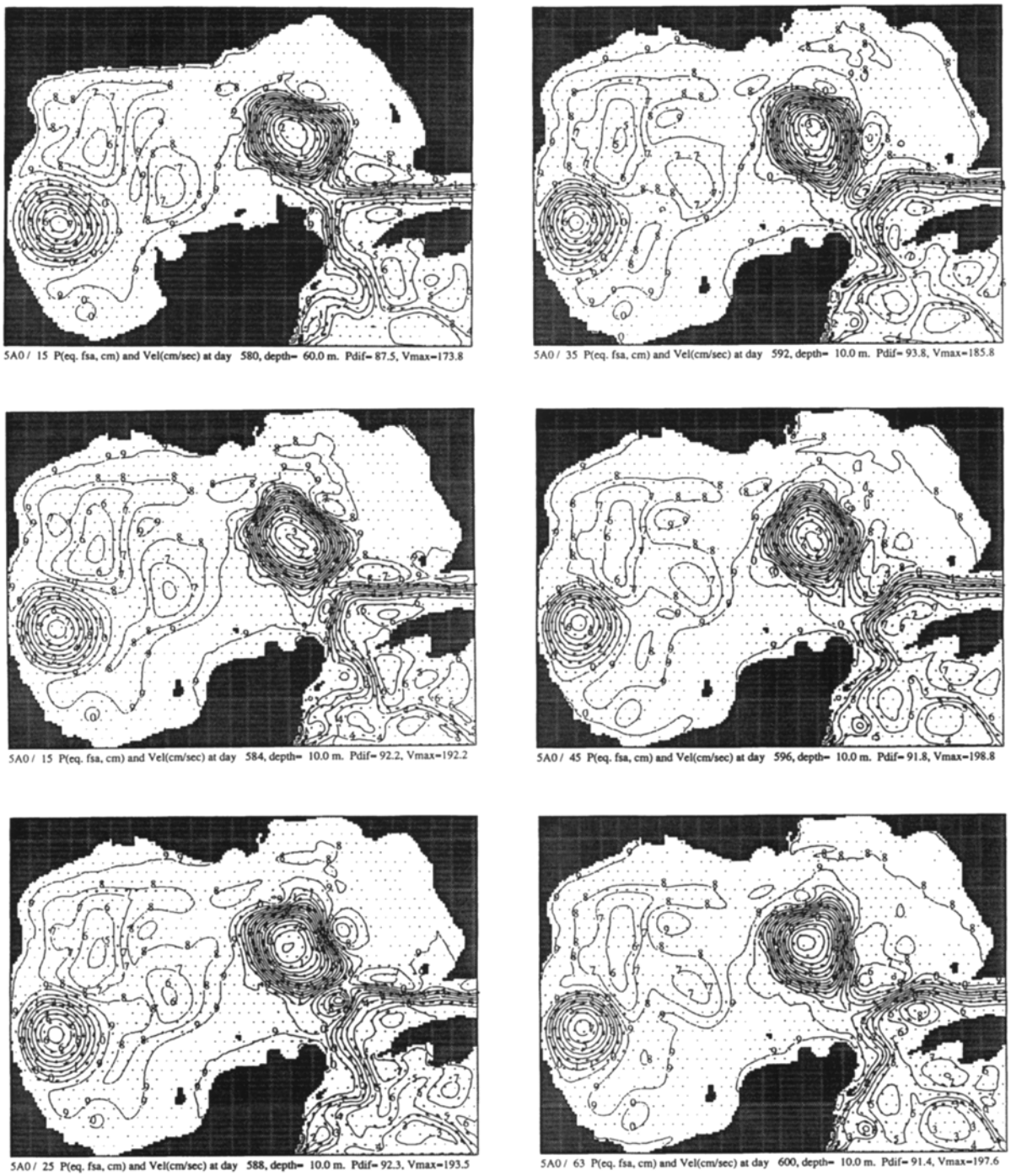

Fig. 7. As Fig. 5, but for the period from days 580 to 600 at 4-day intervals; only the top layer model pressure and velocity fields are shown. Three cold core frontal Loop Current eddies merge during this sequence

northwestern part of the Loop Current in the temperature field on day 1200. Videotape animations, available on request, show the eddy flow very clearly. It is resolved by at least 5 grid points. The occluded pattern is then advected around the head of the Loop Current as the occlusion lengthens. Similar frontal occlusions occur in the atmosphere but involve cold air rather than warm water. Our model simulations show that the cyclonic frontal eddies often pass

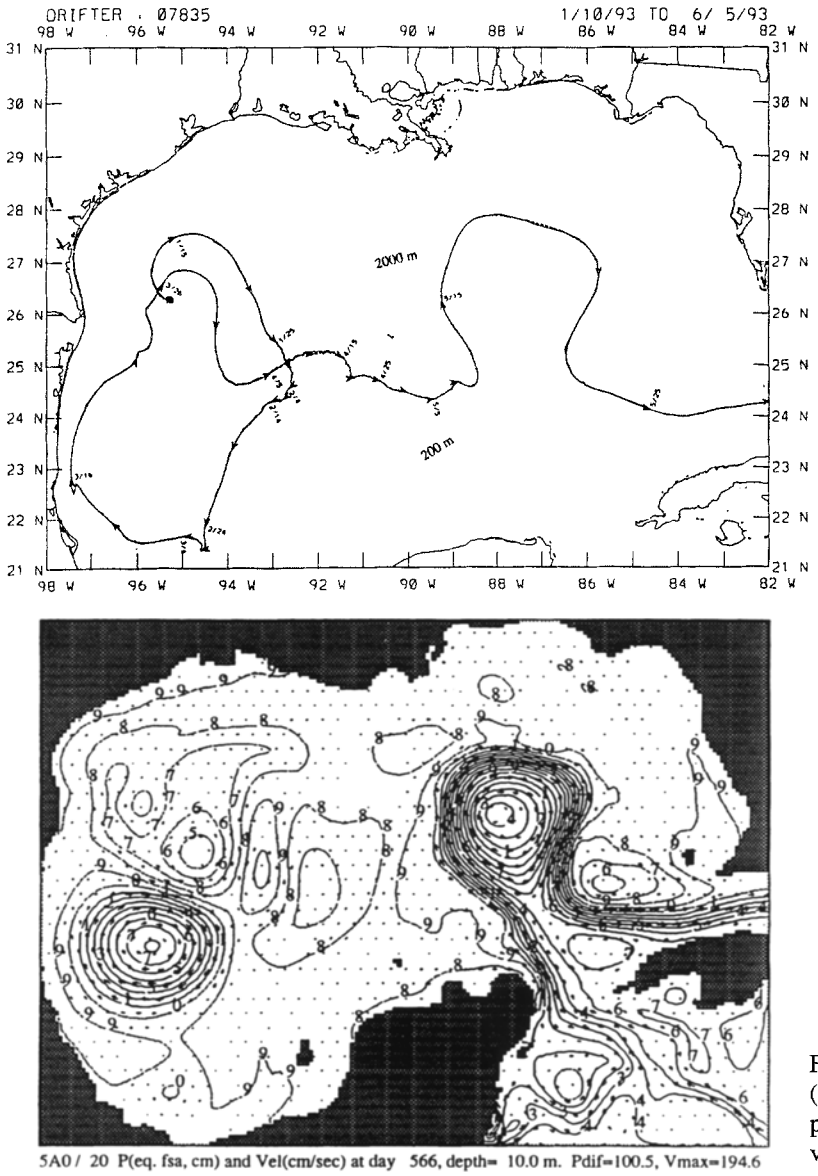

Fig. 8. The top panel shows a drifter trajectory (provided by P. Hamilton, while the bottom panel shows the top layer model pressure and velocity fields at day 566

through the Florida Strait after circling around the Loop Current. At times, they are temporarily trapped off the southwestern Florida shelfbreak so that other frontal eddies being advected around the Loop can merge with them. This concentrates the Loop Current outflow along the northern coast of Cuba (Fig. 5, day 1210). On day 1190, Fig. 5 also shows a small cyclonic eddy east of an old warm core eddy in the extreme western Gulf, as often observed. This reflects the southward movement of large absolute potential vorticity northern Gulf water that has been entrained into the westward moving warm core eddy.

To further examine the small scale phenomena of the Gulf circulation simulated by our model, we show in Figs. 6 and 7 a time sequence from days 500 to 600. Figure 6 shows the top layer model pressure, velocity and temperature from days 500 to 560 at 20-days intervals, while Fig. 7 shows only the pressure and velocity from days 580 to 600 at an interval of 4 days. On days 500 to 520 (Fig. 6), we again see a Loop Current frontal eddy that is trapped off the southwestern Florida shelfbreak, thus focusing the Loop Current outflow along the northern coast of Cuba.

At the same time, two old warm core anti-cyclonic Loop Current eddies merge in the western Gulf during days 500 to 560 (Fig. 6). The fronts from both eddies are quite apparent in this sequence. The sharp kink in the old eddy front at day 540 (Fig. 6) is indicative of the low

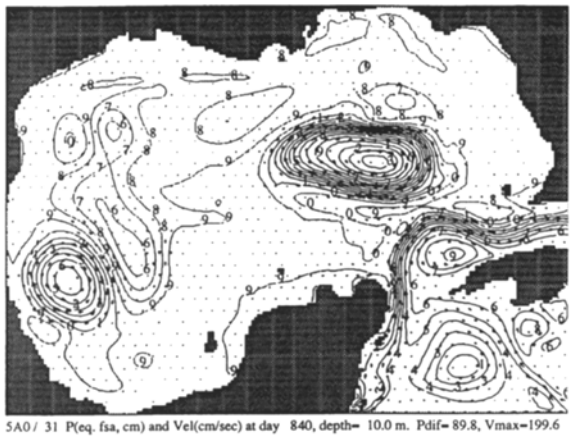

numerical dissipation used in our model. Similar eddy mergings have been reported in the East Australian Current (Cresswell, 1982; Cresswell and Legeckis, 1986). DKY show the major impact of using conventionally (but unphysically) large model dissipation parameters on eddy formation and interaction in the western GOM as well as on Loop Current eddy shedding dynamics. For example, using eddy viscosity of 200 m^2/sec eliminates the formation of parasitic eddies in the western GOM, which are remarkably similar to observations with 20 m^2/sec and even more similar with 2 m^2/sec.

As cyclonic vortex elements enter the Florida Strait, they elongate longitudinally and propagate along the north side of the Strait (Fig. 7, days 580 to 588), as often observed. Three cold core cyclonic Loop Current frontal eddies merge during days 580 to 600. An old anitcyclonic eddy is still clearly evident in the extreme western Gulf. The simulation of such long lived eddies, which are consistent with observations, is possible due to the small numerical dissipation in the model.

The frontal eddies which develop along the Loop Current (Figs. 4 to 7) tend to be spaced about 90° apart around the Loop Current, especially when the latter has penetrated northward into the GOM. As a result, the top layer model pressure contours of the Loop Current often appear like a square with rounded corners, rather than a simple arc or loop. Figure 8 shows such a pattern assumed by a drifter trajectory (Hamilton, 1993), which moved through the Loop Current in about one week. Its pattern is similar to that on day 566 of our model, which is also shown in Fig. 8 for comparison; the trajectory of a numerically simulated drifter entering the model Loop Current on days 520 (Fig. 6) or 1210 (Fig. 5) would show a similar pattern. This pattern rotates as the frontal eddies circle the Loop Current; the model simulations shown in Figs. 5–8 show that this "square with rounded corners" pattern is quite common.

Fig. 9. As Fig. 5, but for days 840 to 900 at 20-day intervals; only the top layer model pressure and velocity fields are shown. The sequence shows the reattachment and final separation of a Loop Current eddy

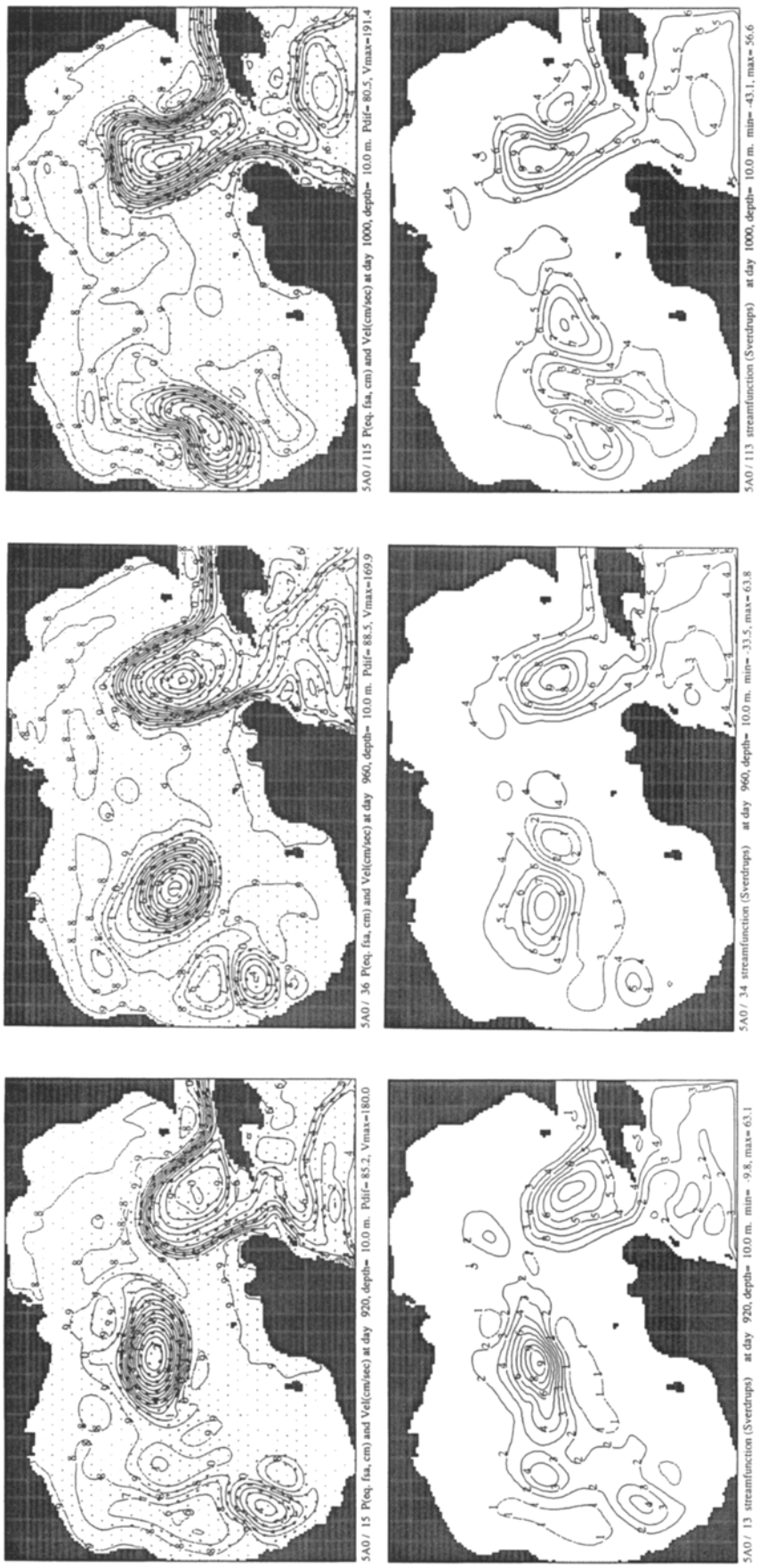

Fig. 10. The left panel shows the top layer model pressure and velocity fields at days 920, 960 and 1000; the right panel shows the vertically integrated streamfunction (Sv). There is an eastward dispersion of the barotropic mode which is not seen at the surface

Parasitic cold core cyclonic eddies are an important part of the dissipation of old warm core Loop Current eddies in the western Gulf (DKY). They often circle around the old warm core eddies, being trapped in the southwestern GOM and leading to a generally cyclonic circulation there. However, they sometimes squeeze between the old warm core eddy and the western GOM Shelf (Fig. 6, days 500–540). Occasionally, a short-lived reverse flow occurs through the Yucatan Strait (figure not shown). The presence of such small scale features in our simulation indicates once again the low dissipation of the DieCAST model.

Figure 9 shows a sequence from days 840 to 900, which depicts the reattachment of a separated Loop Current eddy, followed by its final separation. This reattachment occurs because its elongated pattern is rotated by self-advection. Alternately, frontal eddies on the separated warm core eddy circle the eddy, thus rotating the pattern. Finally, Fig. 10 shows the eastward dispersion of the barotropic mode associated with a shed warm core eddy, as revealed by the wave train in the vertically integrated streamfunction. This leads to multiple barotropic eddies between the principal shed eddy and the Loop Current. This dispersion is not seen in the surface patterns. Near the surface, the baroclinic mode at the surface apparently nearly cancels the barotropic mode in the eastward dispersion. A similar sequences occurs with each major Loop Current eddy shedding cycle. A VHS videotape of the animation of these results is available on request.

4. Concluding Remarks

Our present high resolution results and those of earlier lower resolution studies by DL and DKY show a wide variety of large and small scale phenomena in the GOM that compare well with conventional and satellite data. This dynamic similarity results from realistically small dissipation and the higher order accurate treatment of dominant terms in the governing equations. The use of unphysically large viscosity compromises dynamic similarity to the real ocean. For example, boundary current separation and eddy generation are sensitive to the Reynolds number. The effect of such phenomena on the large scale need not be primarily diffusive. Another diffusive effect is instant convective adjustment, as it is equivalent to the use of an infinite vertical diffusivity. This may not accurately represent the small scale convective plume effects on the large scale environment (Lin and Dietrich, 1994). The use of realistically small dissipation and an accurate treatment of the dominant terms can be just as important as detailed parameterizations of dissipation and other secondary processes.

We have seen that there is a good agreement of the simulated and observed empirical orthogonal functions for the vertical temperature profiles. This result, and the fact that the amplitudes of the empirical orthogonal functions are well correlated with GEOSAT-derived dynamic sea surface heights, indicates that the assimilation of observed sea surface heights into the DieCAST or SOMS model should lead to excellent nowcast/forecast capability in the Gulf of Mexico.

Acknowledgements

We gratefully acknowledge the advice and encouragement provided by Dana Thompson, Harley Hurlburt and Alan Wallcraft during this research. This research was supported by the Office of Naval Research's Navy Ocean Modeling and Prediction Program under Research Grant N00014-92-J-4109 with Mississippi State University, by NSF grants 0CE8911120, OCE8922124, OCE9021904, and 0CE9221756. The use of the computational facilities at Centre de recherche en calculal appliqué (CERCA) in Montreal is acknowledged with thanks.

References

Arrango, H. G., Reid, R. O., 1991: A generalized reduced-gravity ocean model. *Atmos. Ocean,* **29**, 256–287.

Blumberg, A. F., Mellor, G. L., 1985: A simulation of the Circulation in the Gulf Mexico. *Isr. J. Earth Sci.,* **34**, 122–144.

Cresswell, G. R., 1982: The coalescence of two East Australian Current warm-core eddies. *Science,* **215**, 161–164.

Cresswell, G. R., Legeckis, R., 1986: Eddies off southeastern Australia. *Deep-Sea Research,* **33**, 1527–1562.

Dietrich, D. E., Marietta, M. G., Roache, P. J., 1987: An ocean modeling system with turbulent boundary layers and topography: numerical description. *International J. Num. in Fluids*, **7**, 833–855.

Dietrich, D. E., Roache, P. J., Marietta, M. J., 1990: Convergence studies with the sandia Ocean Modeling System. *International J. Num. Methods in Fluids* **11**, 127–150.

Dietrich, D. E., 1992: The Sandia Ocean Modeling System Programmers Guide and Users Manual, SAND93-7386. SAND92-7386 Sandia National Laboratories, Albuquerque, NM 87185.

Dietrich, D. E., Lin, C. A., 1994: Numerical studies of eddy shedding in the Gulf of Mexico. *J. Geophys. Res.,* **99**, 7599–7615.

Dietrich, D. E., Ko, D.-S., 1994: A semi-collocated ocean model based on the SOMS approach. *International J. Num. Methods in Fluids,* **19**, 1,103–1,113.

Dietrich, D. E., Ko, D.-S., Yeske, L. A., 1994: On the application and evaluation of the relocatable DieCAST ocean circulation model in coastal and semi-enclosed seas. Technical Report 93-1, Center for Air Sea Technology, Mississippi State University, Stennis Space Center, MS 39529-6000.

Hamilton, P., 1993: Hydro/drifter data at shelf edge. LATEX III Meeting, October 27–28, 1993, New Orleans, LA.

Haney, R. L., 1971: Surface boundary condition for ocean circulation models. *J. Phys. Oceanogr.,* **1**, 241–248.

Haney, R. L., Dietrich, D. E., 1996: A model simulation of wind and boundary forced jets in the coastal ocean off central California, Proceedings of the 76th American Meteorological Society Annual Meeting, Atlanta, GA, 28 Jan–2 Feb, 1996 (invited presentation, with color cover feature).

Hellerman, S., Rosenstein, M., 1983: Normal monthly windstress over the world ocean with error estimates. *J. Phys. Oceanogr.,* **13**, 1093–1104.

Hurlburt, H. E., Thompson, J. D., 1980: A numerical study of Loop Current instrusions and eddy shedding. *J. Phys. Oceanogr.,* **10**, 1611–1651.

Ko, D.-S., 1992: Synthetic temperature profile in the Gulf of Mexico: Part 1. Statistical relationship between model amplitudes and dynamic height at surface. Institute for Naval Oceanography report TM-8.

Levitus, S., 1982: Climatological atlas of the World Ocean. NOAA Prof. Paper 13, U.S. Dep. of Commerce, Washington, D.C., 173 pp.

Lewis, J. K., Kirwan, A. D., Jr., 1987, Genesis of a Gulf of Mexico ring as determined from kinematic analysis. *J. Geophys. Res.,* **92**, 11,727–11,740.

Lewis, J. K., Hsu, S. A., 1992: Mesoscale air-sea interactions related to tropical and extratropical storms in the Gulf of Mexico. *J. Geophys. Res.,* **97** (C2), 2215–2228.

Lin, C. A., Dietrich, D., 1994: A numerical study of low Reynolds number 2-dimensional convective adjustment. *Geophys. Astrophys. Fluid Dyn.,* **74**, 123–134.

Schmitz, W. J., Richardson, P. L., 1991: On the sources of the Florida Current. *Deep Sea Res.,* **38**, S379–S409.

Smith, D. C., IV, 1986: A numerical study of Loop Current eddy interaction with topography in the western Gulf of Mexico. *J. Phys. Oceanogr.,* **16**, 1260–1272.

Vukowich, F. M., Maul, G. A., 1985: Cyclonic eddies in the Eastern Gulf of Mexico. *J. Phys. Oceanogr.,* **15**, 105–117.

Wallcraft, A. J., 1986: Gulf of Mexico circulation modeling study, Annual progress report: Year 2, Report to Minerals Management Service, 94, pp. JAYCOR, Vienna, Va.

Authors' addresses: David E. Dietrich, Center for Air Sea Technology, Mississippi State University, Stennis Space Center, MS 39529-6000, U.S.A.; Charles A. Lin, Department of Atmospheric and Oceanic Sciences and Centre for Climate and Global Change Research, McGill University, Montreal, P.Q. Canada H3A 2K6; Dr. Alberto Mestas-Nunez, CIMAS, University of Miami, 4600 Rickenbacker Causeway, Miami, FL 33149, U.S.A.; Dong-Shan Ko, Sverdrup Technology, Building P110, Stennis Space Center, MS 39529, U.S.A.